Contents lists available at ScienceDirect

Journal of Pharmaceutical Sciences

journal homepage: www.jpharmsci.org

Check for updates

Effect of Azide Preservative on Thermomechanical Aggregation of Purified Reference Protein Materials

Sean E. Lehman [a], Ioannis Karageorgos [a], Jeremy R. Filteau [a, b], Wyatt N. Vreeland [a, *]

[a] Biomolecular Measurement Division, Bioprocess Measurements Group, National Institute of Standards and Technology, Gaithersburg, MD 20899, USA
[b] Department of Chemical Engineering, University of Washington, Seattle, WA 98195, USA

ARTICLE INFO

ABSTRACT

Protein aggregation can affect the quality of protein-based therapeutics. Attempting to unravel factors influencing protein aggregation involves systematic studies. These studies often include sodium azide or similar preservatives in the aggregation buffer. This work shows effects of azide on aggregation of two highly purified reference proteins, both a bovine serum albumin (BSA) as well as a monoclonal antibody (NISTmAb). The proteins were aggregated by thermomechanical stress, consisting of simultaneous heating of the solution with gentle agitation. Protein aggregates were characterized by asymmetric flow field flow fractionation (AF^4) with light scattering measurements along with quantification by UV spectroscopy, revealing strong time-dependent generation of aggregated protein and an increase in aggregate molar mass. Gel electrophoresis was used to probe the reversibility of the aggregation and demonstrated complete reversibility for the NISTmAb, but not so for the BSA. Kinetic fitting to a commonly implemented nucleated polymerization model was also employed to provide mechanistic details into the kinetic process. The model suggests that the aggregation of the NISTmAb proceeds via nucleated growth and aggregate-aggregate condensation in a way that is dependent on the concentration (and presence) of the azide anion. This work overall implicates azide preservatives as having demonstrable effects on thermomechanical stress and aggregation of proteins undergoing systematic aggregation and stability studies.

Published by Elsevier Inc. on behalf of the American Pharmacists Association. This is an open access article under the CC BY-NC-ND license (http://creativecommons.org/licenses/by-nc-nd/4.0/).

Introduction

Protein agglomeration and aggregation are important degradation pathways for biotherapeutics and have been studied in detail for monoclonal antibodies.[1–3] Aggregation of normally functioning endogenous proteins can lead to pathologies such as in amyloidosis, Huntington's disease, Alzheimer's, and Lou Gehrig's disease. There are increasing requirements from regulatory bodies to detect and quantify aggregated proteins in therapeutic treatments.[4] The driving interest in aggregation of therapeutic agents stems from increasing concern around adverse reactions related to the presence of aggregated therapeutics during administration in clinical settings.

Current work in the field focuses on extensive characterization and determination of underlying aggregation mechanisms.[5–7] These endeavors focus on directed aggregation, where proteins are aggregated reproducibly to a certain extent by systematically controlling (and ultimately understanding effects of) solution parameters including pH, ionic strength, temperature, buffer composition, etc.[8,9] This helps expand knowledge around what conditions drive protein aggregation, thereby guiding approaches to minimize the aggregation of therapeutic molecules. Another key approach involves understanding how minor perturbations during all aspects of the therapeutic production and certification process can ultimately lead to generation of aggregated clinical therapeutic agents with the adverse clinical outcomes described above.[10,11]

A common factor included in many of these explorations is the inclusion of a buffer containing a biological preservative-such as sodium azide-at low levels (i.e. mg per liter a.k.a. parts per million [ppm] concentration). Sodium azide is bacteriostatic due to its ability to bind strongly to the cytochrome c oxidase iron (II) center, which most bacteria rely on for energy generation.[12] An unresolved

question is what, if any, effects the presence of this preservative has on aggregation. Since it is present at very low levels ($\approx$ 3 mmol/L), the consensus has been that its effects are negligible on aggregation.[13-15] Initial experimental observations in our laboratory concerning protein aggregation implied aggregation of otherwise stable immunoglobulins did not appear to proceed in the absence of azide (in the aggregation buffer). The aggregation buffer is taken to be the buffer in which the protein is dissolved during systematic aggregation studies through various stressors. This was discovered by accidental inclusion/exclusion of the azide in the buffer. Accelerated aggregation was observed with the inclusion of the azide, whereas only minimal aggregation was observed when the azide was excluded. These observations concerning the possible effect of azide on thermomechanical aggregation (consisting of a combination of thermal stress and gentle mechanical agitation) ultimately led to the work reported herein.

In this work, reference proteins were aggregated under systematically controlled conditions using a combination of thermal and mechanical stress. Sodium azide, a common preservative, was included at varying concentrations to understand its effects on the aggregation process. The protein aggregates were fractionated by asymmetric-flow field flow fractionation (AF[4]) and are characterized by multi-angle light scattering (MALS) measurements. This enables characterization of the aggregate size and molar mass, as well as the fraction of monomeric and aggregated protein. Additionally, the aggregates were characterized by polyacrylamide gel electrophoresis under both native and reducing conditions. Electrophoresis of the protein aggregates enables understanding the degree of reversibility of the aggregation process. Kinetic analysis of the evolution of aggregated protein species facilitates extraction of key kinetic parameters based on fitting to the Lumry-Eyring nucleated polymerization (LENP) aggregation model, providing insight into the mechanisms of the aggregation process and the effects of the azide preservative on said processes. This work overall gives a robust framework for understanding unintended effects of biological preservatives on aggregation processes as well as outlining a general methodology for preparation and characterization of sub-visible soluble aggregates of highly purified proteins.

Materials and Methods*

*Certain commercial reagents and instrumentation are identified throughout to adequately describe the experimental procedures. In no case does such an identification imply an endorsement by NIST, nor does NIST suggest that the materials or equipment so identified are necessarily the best available for the purposes described herein.

Protein Sample Preparation and Aggregation

Phosphate buffered saline, 10 mM at pH = 7.4 (PBS) was prepared by dissolving the premeasured buffer salts (Sigma-Aldrich, St. Louis, MO, SKU P3813) in deionized (18.2 M$\Omega\bullet$cm resistivity) water prepared by an in-house MilliQ system (MilliporeSigma, Burlington, MA) to give the buffer solution. A histidine buffer containing 12.5 mmol/L L-histidine (His) and 12.5 mmol/L L-histidine hydrochloride monohydrate (HisHCl) (Sigma-Aldrich, St. Louis, MO, His SKU H8000; L-HisHCl SKU 53370), was prepared by dissolving the dry powders into the same deionized water as above to give a pH = 6.0 buffer. Sodium azide was obtained as a solution of mass concentration of 5% in water from Ricca Chemical Co. (Arlington, TX, USA). (*Safety Note Sodium azide is highly toxic; risks are mitigated by using a commercially prepared solution rather than dissolving the powdered reagent into solution; this minimizes particulate*

aerosolization of the reagent.) Buffer solutions were passed through a 0.02 μm poly (ethersulfone) filter immediately before use.

NIST candidate Standard Reference Material (SRM) 927f Bovine Serum Albumin, of mass concentration 7% in water, (hereafter referred to as BSA) and NISTmAb Primary Sample (PS) 8670 (hereafter referred to as NISTmAb) were obtained from the National Institute of Standards and Technology. NISTmAb was supplied in frozen vials at nominal concentration 100 mg/mL in formulation buffer consisting of 12.5 mmol/L L-histidine, 12.5 mmol/L L-histidine HCl (pH 6.0).[16] Both BSA and NISTmAb were diluted to 10 mg/mL final concentration in the PBS and His/His-Cl buffers, respectively, as described above. The sodium azide solution was added during the dilution process to either the PBS or His/His-Cl buffers (not containing azide) during preparation to yield final concentrations of 0 mmol/L (0 ppm), 1.54 mmol/L (100 ppm), 3.08 mmol/L (200 ppm), or 6.15 mmol/L (400 ppm) of sodium azide (by dilution of volume into volume). These concentrations were selected as they are the concentrations most typically used for preservative purposes. Protein solutions (10 mL total volume at 10 mg/mL nominal protein concentration) were prepared in 20 mL glass scintillation vials with polypropylene caps and a polyethylene cone liner that forms the seal (used as received, #66022-065 VWR International, Radnor, PA). Protein solutions once prepared were not filtered to preclude protein loss by adsorption onto filter membranes. All protein samples were aggregated on the same day that they were prepared. Proteins in solution were aggregated by thermal and physical perturbation via constant end-over-end rotation at three revolutions per minute in a Robbins Scientific Model 400 hybridization oven. BSA was incubated at 65 °C and NISTmAb was incubated at 75 °C. These temperatures were selected to be near the first irreversible melting temperature as reported in the literature.[17,18] The sample was placed in the oven and the rotation turned on, then 10 min were allowed to elapse before starting the clock. This initial thermal delay of 10 min under rotation was included to allow the protein solution to come to thermal equilibrium with the oven. It was experimentally determined that the temperature increase was approximately 40 °C over the course of the thermal delay. At each hour time point, the vial was removed from the hybridization oven and 1.00 mL of the protein solution was transferred into a glass autosampler vial (Agilent Technologies, Santa Clara, CA). The sample aliquot was immediately quenched into an ice-water bath and held for 10 min to cool the solution. All samples were stored at 4 °C in autosampler vials until analysis, which occurred on the same day the samples were aggregated.

Asymmetric-Flow Field Flow Fractionation (AF[4])

An Eclipse DualTec AF[4] system (Wyatt Technology, Santa Barbara, CA) was coupled inline to a UV/Vis diode array detector (Model 1260, Agilent Technologies, Santa Clara, CA), a HELEOS-II multiangle laser light photometer, and an Optilab T-Rex differential refractive index detector (Wyatt Technology). The AF[4] channel was a vendor-supplied "short" channel with 350 μm thick "wide" (Mylar) spacer; an Ultracel 10 kDa regenerated cellulose (Millipore, Burlington, MA) ultrafiltration membrane served as the accumulation wall. Samples were introduced into the AF[4] separation channel via an Agilent 1260 autosampler (Santa Clara, CA) with a focus position of 12% of the channel length. The focusing was accomplished by flowing 0.2 mL/min of buffer into the channel inlet and 1.3 mL/min of buffer through the channel outlet for 5 min. After the samples were introduced and focused against the ultrafiltration membrane, they were eluted from the column in a size selective manner with a channel flow of 1.0 mL/min while the cross flow was linearly ramped from 3.0 mL/min to 0 mL/min over 45 min. Post separation the channel was rinsed for 5 min with

1.0 mL/min channel flow and 0 mL/min crossflow and the injector "on" to rinse out the sample loop.

Monomer/Aggregate Fraction Measurement and Aggregate Molar Mass Distribution

As the sample eluted from the AF[4] channel, it was fed into the UV−Vis detector where the concentration of the eluting fractions was determined using a mass extinction coefficient of 0.679 mL/mg•cm (BSA) and 1.4 mL/mg•cm (NISTmAb) for both the monomeric protein and the protein aggregate. The amount of monomer in each sample was determined by integrating the area under the peak representing the monomer using ASTRA 7.3.2 software (Wyatt Technology). The eluted fraction next flowed into the HELEOS detector where the flow cell was illuminated with a plane-polarized laser ($\lambda = 662$ nm) and the scattering intensity was measured at 16 different angles simultaneously. The scattering data were fitted with Zimm formalism (neglecting second virial coefficient effects and assuming the aggregates are much smaller than the wavelength of incident light) the scattering intensity at zero angle was extrapolated and the molar mass determined according to Equation (1):

$$M = \frac{R(0)}{K\,c} \tag{1}$$

here M is the molar mass of the eluting fraction, c is the concentration measured by the UV−Vis detector, $R(0)$ is the extrapolated scatter intensity at $0°$ angle and K is the instrument constant described by Equation (2):

$$K = \frac{4\pi^2 \left(\frac{dn}{dc} \right)^2 n^2}{N_{AV} \lambda^4} \tag{2}$$

where $\frac{dn}{dc}$ is the change in the refractive index of the solution with a change in solute concentration, n is the solvent refractive index, N_{AV} is Avogadro's number, and λ is the wavelength of light. Extrapolation and calculations were done with ASTRA 7.3.2 software.

Native and Denaturing Polyacrylamide Gel Electrophoresis (PAGE)

BSA and NISTmAb protein samples (consisting of monomeric and aggregate protein) at 5 µg/µL were resolved on 6% PAGE gel and 12% PAGE gels, respectively. Each well of the gel was loaded with 20 µL of each sample. The samples for both BSA and NISTmAb was comprised of 10 µL of protein sample (at concentration 3 µg/µL) plus 10 µL of the loading buffer. Electrophoresis was carried out under either reducing conditions with sodium dodecyl sulfate in the buffer (with samples incubated at 70 °C for 5 min in Laemmli buffer containing 5% β-mercaptoethanol) or under native conditions (absence of sodium dodecyl sulfate (SDS) and β-mercaptoethanol). Protein bands in the gels were visualized using Coomassie blue (Bio-Rad, Hercules, CA) stain. For reductive alkylation the proteins were buffer exchanged into 100 mmol/L Tris-HCl, pH 8.3. Then proteins were incubated in 8 mol/L guanidine hydrochloride [(GdnHCl), (Thermo Scientific)] for 20 min. An aliquot of 0.5 mol/L stock solution tris(2-carboxyethyl)phosphine hydrochloride [(TCEP) (Sigma Aldrich)] was added to a final concentration of 5 mmol/L and incubated for 30 min at 56 °C. The protein mixture was then cooled to room temperature for 30 min and iodoacetamide [(IAA), (Sigma Aldrich) (0.5 mol/L stock solution)] was added to a final concentration of 14 mmol/L. The mixture was incubated

for 30 min at room temperature in the dark. Samples were buffer exchanged into PBS to remove residual TCEP, IAA and GdnHCl.

LENP Model Differential Equation Fitting

The measured monomer concentrations and molar mass of aggregate were appropriately normalized, then Equations (4−7) were fit using in-house written Python code (https://www.python.org) that was developed in Spyder (https://www.spyder-ide.org) using NumPy scientific development package (https://numpy.org) and the symfit module (https://pypi.org/project/symfit/).[19] After fitting to extract the characteristic time constants, the normalized data were transformed back into units that matched the experimentally measured quantities and plotted against the experimentally measured data in OriginPro 9.65 (OriginLab Corporation, Northampton, MA). The error of the fit parameters was assumed to be experimental error (calculated at 1σ) and not as relative weights for the fitting parameters.

Inductively Coupled Plasma-Mass Spectrometry (ICP-MS) of Sodium Azide Solution

From a single sub-sample of a mass concentration of 5% sodium azide in water, subsamples of nominal mass 0.05 g, 0.16 g, and 0.30 g were weighed by difference into clean 60 mL LDPE Nalgene bottles (02-924-6B, Fisher Scientific, Hampton, NH) which had been washed with a volume fraction of 15% nitric acid in water. Following this, a nominal 1 g subsample of a 101.78 µg/kg solution of indium in a volume fraction of 2% nitric acid in water was added to each of the three subsamples to serve as an internal standard. One procedure blank was processed in like manner, except no stock solution of sodium azide was added. Samples were diluted to 50 g total mass with a volume fraction of 2% HNO_3 in water, resulting in nominal dilution factors of 1000, 316 and 163, for sub-samples 1, 2, and 3, respectively. In all cases, exact masses were obtained on an analytical balance with readability of 0.02 mg and recorded electronically.

Calibrant solutions were prepared by mixing two multielement stock solutions and the indium internal standard solution. The first multielement stock solution contained: antimony, hafnium, molybdenum, silicon, silver, tin, titanium, tungsten and zirconium. The second multielement stock solution contained: aluminum, arsenic, barium, beryllium, bismuth, cadmium, chromium, cobalt, copper, europium, gallium, germanium, holmium, iron, lanthanum, lead, lithium, magnesium, manganese, nickel, phosphorus, selenium, sodium, strontium, thallium, thorium, uranium vanadium, ytterbium and zinc. Calibrant solutions were prepared to contain nominally 2 µg/kg In and 0.1 µg/kg, 1 µg/kg, 2 µg/kg and 10 µg/kg of each element in a volume fraction of 2% HNO_3 in water.

Mass spectrometric analyses were performed on the Thermo XSERIES 2 ICP-MS (Waltham, MA) equipped with matrix tolerant (Xt) cones operated at 1400 W. Solutions were introduced via a peristaltic pump into a low flow (100 µL/min) PFA micro-concentric nebulizer. The nebulizer was fitted to an impact-bead spray chamber cooled to 2 °C. ICP-MS operating parameters were optimized using a tune solution containing lithium, indium, cerium, and uranium. Tune parameters were adjusted per manufacturer specifications to obtain maximum sensitivity for ^{115}In and a$^{156}CeO^+/^{140}Ce^+$ ratio less than 2%. Sample measurements were made using scan mode at standard resolution with 25 channels per atomic mass unit. Data were acquired at 0.3 ms per channel for one hundred sweeps, yielding 60 s of data per scan. Five, 60 s scans were acquired per sample. Samples were analyzed sequentially from high to low dilution using an autosampler fitted with a 0.25 mm i.d. probe. An acid solution of volume fraction 2% HNO_3 in
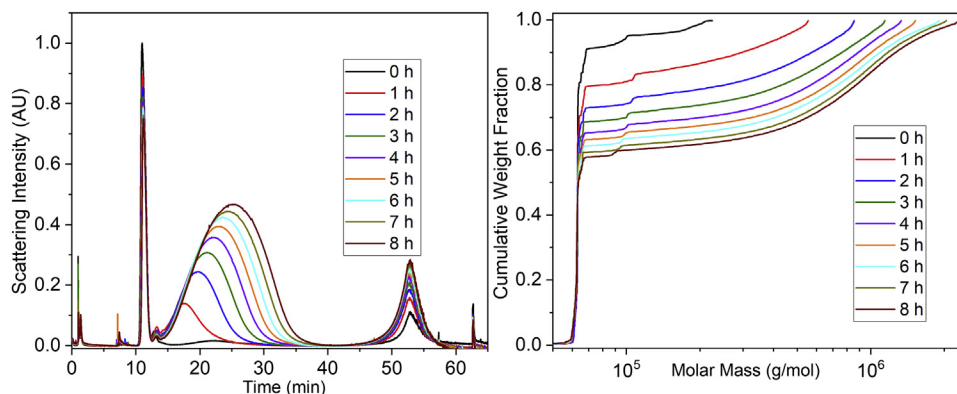
Fig. 1. (L): Light scattering intensity at 90° as a function of chromatographic separation time for BSA at 10 mg/mL with 200 mg/L NaN₃. (R): Molar mass distribution as a function of aggregation time for the same BSA sample.

water was used as a wash between samples. Element mass fractions were quantified using the generated external calibration curve. Signal drift was corrected versus the In internal standard. Low, medium and high level calibrant solutions were run as samples to check for carry-over and drift. The limit of quantitation (LOQ), defined as the concentration at ten times the standard deviation of the signal for a blank sample, was less than 1 μg/kg for all elements except iron and selenium, each with LOQ of less than 10 μg/kg.

Results and Discussion

Aggregation of BSA (Candidate SRM 927f)

The light scattering signal at 90° collection angle of the AF⁴-MALS separation of BSA aggregated at 65 °C is shown in Fig. 1 (left panel) over time from zero hours through 8 h in 1-h increments. Particles and/or molecules move through the AF⁴ channel in a size-dependent manner from smallest to largest, when operated in normal mode. The narrow peak located around 12 min represents free protein monomer that passes most rapidly through the fractionation system. The broad peak starting at 15 min and extending up to as much as 40 min represents the aggregated protein. As can be seen at an incubation time of zero hours, the monomer peak is at its maximum and there is minimal aggregate present in the fractogram (<10%). As the protein sample is thermally stressed with gentle agitation, substantial protein aggregate can be detected after 1 h. As the aggregation proceeds, an increase in the amount of aggregate, as well as a concurrent shift to longer elution times as the overall molecular weight of the aggregate increases over time.

As the amount and molar mass of the aggregate fraction begins to grow, a concurrent decrease in the amount of monomer can also be seen. Following 8 h of thermal aggregation, the amount of BSA monomer decreases from an initial 90% monomer to approximately 55% residual monomer following 8 h. The broad peak at approximately 50 min represents larger aggregates that are present at minimal mass concentration and were excluded from the data analysis. In this size regime the intensity of light scattering scales with particle radius to the sixth power; this highly non-linear effect greatly magnifies the appearance of a small mass of material that is larger in size than the other particles in the sample. Thus, these low mass-abundance aggregates were neglected in the analysis.

From the MALS analysis, the molar mass distribution of the BSA can be calculated (Fig. 1, right panel). At zero hours of incubation effectively all sample shows a calculated molecular weight of 65 kDa, which corresponds to the molar mass of BSA monomer. The zero hour time point represents protein that was diluted into the azide buffer but was never exposed to the thermomechanical conditions. As the aggregation proceeds, a shift can be seen in the fraction of the monomer as well as a marked increase the molar mass of the aggregate. As the monomer peak does not shift throughout the time series, the characteristic, reproducible peak around 14 min (Fig. 1, left) was taken to be the monomeric species. All protein under this peak was calculated to be monomeric for the purposes of analysis. The peak starting at around 14 min until around 40 min is considered "aggregate." This intrinsically includes dimeric, trimeric, and all higher-order species. For the BSA sample, the aggregation appears to proceed independent of the azide concentration (Fig. 2, left). The monomer concentration as a
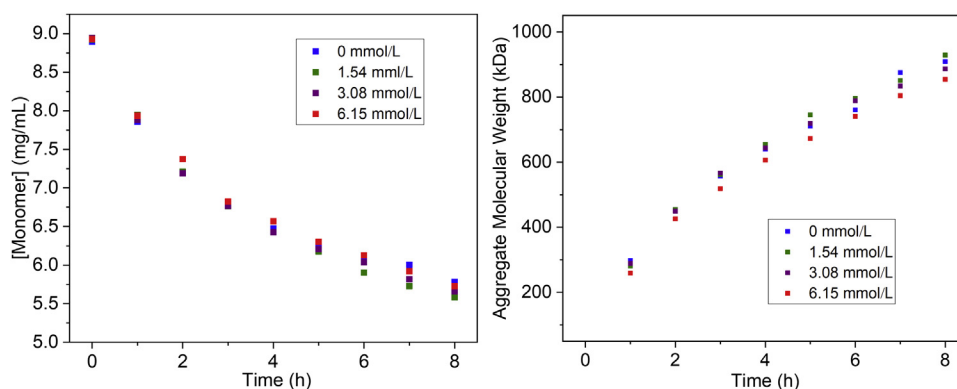

Fig. 2. (L): BSA monomer concentration as a function of aggregation time and azide concentration, quantified by UV spectroscopy. (R): Aggregate BSA molecular weight as a function of aggregation time and azide concentration, quantified by multi-angle light scattering. Data points are experimentally measured values.
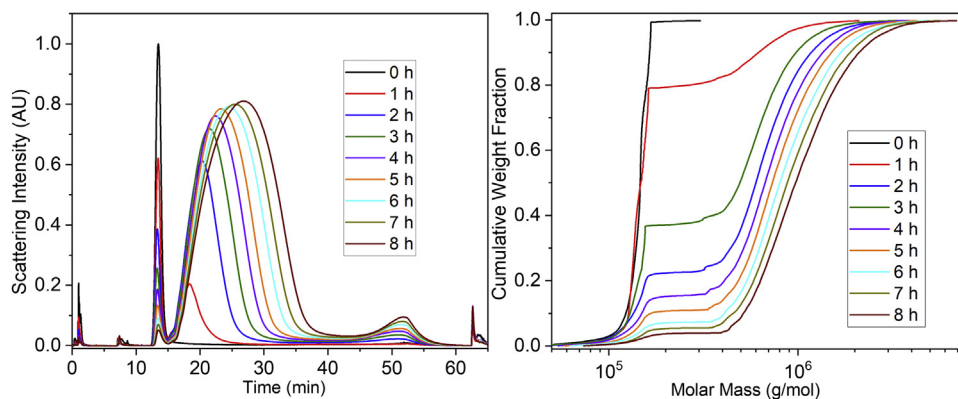
Fig. 3. (L): Light scattering intensity at 90° collection angle as a function of chromatographic separation time during field flow fractionation for aggregated NISTmAb at 10 mg/mL with 200 mg/L NaN$_3$. (R): Cumulative weight fraction as a function of aggregation time of the NISTmAb aggregates.

function of time and azide concentration is shown and while some variation is apparent, the differences do not appear systematic. From this, it can be concluded that the azide concentration does not affect the BSA aggregation.

The molar mass of the aggregate protein was calculated from the portion of the fractogram representing it (as described above) where the exact molar mass at each time point was calculated from Equation (1). The weight average was then calculated via Equation (3):

$$M_w = \frac{\sum_i M_i^2 \, N_i}{\sum_i M_i \, N_i} \qquad (3)$$

where M_i is the molar mass of each fraction and N_i is the number of molecules in each fraction. The effect of the azide concentration on the aggregate mass (M_w, weight-average moment of the distribution) also appears to be minimal (Fig. 2, right). This is to be expected as no effect on the extent of aggregation was observed. Thus, the calculated average molar mass of the aggregate varies with time but not the azide concentration.

Aggregation of NISTmAb (PS 8670)

NISTmAb was also aggregated following the same general protocol as used in the BSA aggregation except for the different temperature of aggregation. The corresponding AF^4-MALS separation

and analysis of the NISTmAb is shown by the stacked fractograms in Fig. 3 (left). This aggregation also took place over 8 h, but at a slightly higher aggregation temperature of 75 °C. The aggregation over time from zero hours through 8 h shows a much more pronounced decrease in the amount of residual monomer when compared to the BSA. The narrow peak at approximately 14 min represents free monomer that passes rapidly through the fractionation system. The broad peak from starting at 15 min and extending up to as much as 40 min represents the aggregated protein. As can be seen at an incubation time of zero hours, the monomer peak is at its maximum and there is minimal aggregate present in the fractogram (<10%). As the aggregate fraction/mass begins to grow, concurrent decrease in the overall magnitude of the monomer peak can also be seen. Following 8 h of thermal aggregation most of the NISTmAb monomer has been converted into aggregate with only 10% monomer remaining. The broad peak at approximately 50 min represents larger aggregates and/or injected particulates, present at minimal concentration, which were excluded from the data analysis as was done with the BSA analysis.

From the MALS analysis, the molar mass distribution of the NISTmAb can also be calculated (Fig. 3, right panel). At zero hours of incubation effectively all sample is at the expected molar mass of NISTmAb (150 kDa). As the aggregation proceeds, the molar mass of the aggregate markedly increases. For the NISTmAb sample, however, the aggregation appears to depend on the azide concentration (Fig. 4, left). The monomer concentration as a function of time and azide concentration is shown and does change in a consistent,
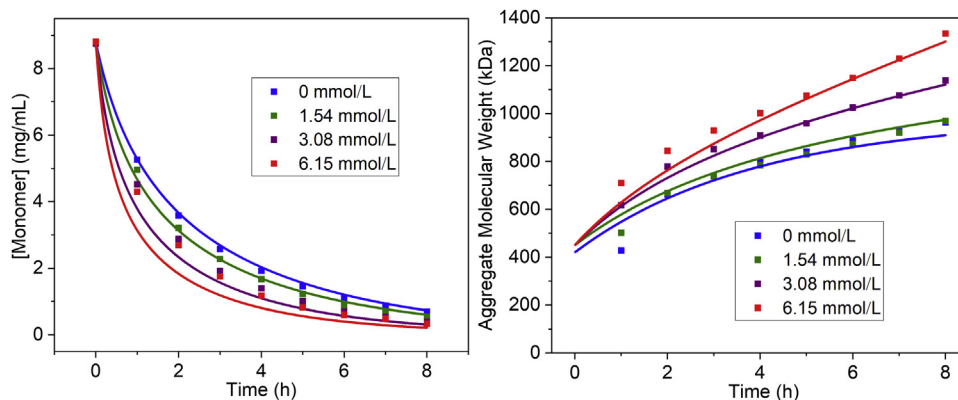

Fig. 4. (L): Kinetic fitting by LENP model to the NISTmAb aggregation results as a function of the monomer concentration over the aggregation time. (R): Kinetic fitting by LENP model to the NISTmAb aggregation results as a function of the monomer concentration over time. Data points are experimentally measured values, the curves are derived from the LENP fitting protocol.

systematic way. The increasing azide concentration accelerates the reaction (resulting in more rapid loss of monomer) and increases the molar mass of aggregated NISTmAb. From this, it can be concluded that the azide concentration does systematically affect the aggregation of the antibody. The effect of the azide concentration on the aggregate mass also is marked (Fig. 4, right), although it is interesting to note that there is effectively no difference of the aggregate molar mass between the no azide condition and the lowest implemented concentration (100 mg/L). The monomer loss does shift with the introduction of the azide. However, once the azide concentration is $\geq$ 200 mg/L, a clear effect on the molar mass of the aggregate over time is apparent from the data. It is somewhat puzzling that the monomer concentration is azide-dependent but that addition of 100 mg/L NaN_3 does not affect the molar mass of the aggregate in any appreciable way. It can be inferred that there is an insufficient molar amount of azide in the 100 mg/L sample to kinetically accelerate the aggregation growth, such that the monomer decreases based on the added azide, but the agglomeration of the growing aggregates is unaffected by the additional azide in the system.

Gel Electrophoresis of Aggregated Proteins

Gel electrophoresis of the aggregates was carried out to test the reversibility of the aggregation process. Native gel electrophoresis neither reduces disulfide bridges nor denatures the protein. Thus, the intact protein runs through the gel according to both its size and charge. In Fig. 5, the electrophoresis data for BSA under native conditions can be seen on the left. The monomer present across the time series is observed as a strong band corresponding to the 65 kDa mass of monomeric BSA (under reducing conditions, right panel). As around half of the intact monomer remains after the aggregation process, this large monomer band was expected. Additionally, extra bands of larger molecular weight are visible. These protein bands are higher order aggregates of varying molecular weight that migrate into the gel. Under reducing and denaturing conditions proteins are unfolded and become uniformly charged via interaction with SDS surfactant. Then proteins migrate primarily according to the overall molecular weight. In addition, the reduced samples were treated with iodoacetamide, which reacts irreversibly with free (*i.e.* reduced) cysteine residues to inhibit cysteine reoxidation. The reducing gel following iodoacetamide treatment is shown on Fig. 5 on the right. As can be seen, most of the protein monomer is recovered at the approximately 65 kDa mass expected. The bands are heavy due to overloading of the gel, but there is less overall protein visible at the higher molecular weight bands compared to the non-reducing gel. Presence of some level of higher molecular weight bands demonstrates that some fraction of aggregate is not converted into monomer during the reduction and capping process.

Electrophoresis of the NISTmAb, however, proceeded very differently. In the case of the non-reducing, no-surfactant PAGE gel (Fig. 6, left panel) the non-thermally stressed material (Lane 0) shows a single band at a molar mass of approximately 150 kDa. This sample was not subjected to the thermal/mechanical aggregation conditions, and so only a single band of the NISTmAb monomer was visualized. As the aggregation proceeded bands of both monomer and very high molecular weight aggregates appear near the edge of the resolving gel (Lanes 1–8). For the resolving gel at 12% acrylamide, proteins larger than approximately 200 kDa will be unable to pass through the acrylamide network and thus will be excluded at the top of the gel, as observed. In contrast when the sample is reduced and alkylated the large molar mass was not seen and only bands of 50 kDa and 25 kDa are observed at all time-points in the thermal stress series. This also is observed for the unstressed sample (Lane 0). Structurally, an immunoglobulin G (IgG) consists of two heavy chains that are linked by disulfide bridges that are also in turn linked to two light chains by disulfide bridges. Complete reduction (and subsequent alkylation, rendering the reduction irreversible) liberates two heavy chains (50 kDa each) and two light chains (25 kDa each). Thus, the total monomeric mass (approximately 150 kDa) is recovered in this experiment by visualization of only the heavy and light chain bands expected from complete cleavage of the disulfide bonds. Because the reduction and subsequent electrophoresis results in only the expected light and heavy chain bands, the aggregation process appears to be completely
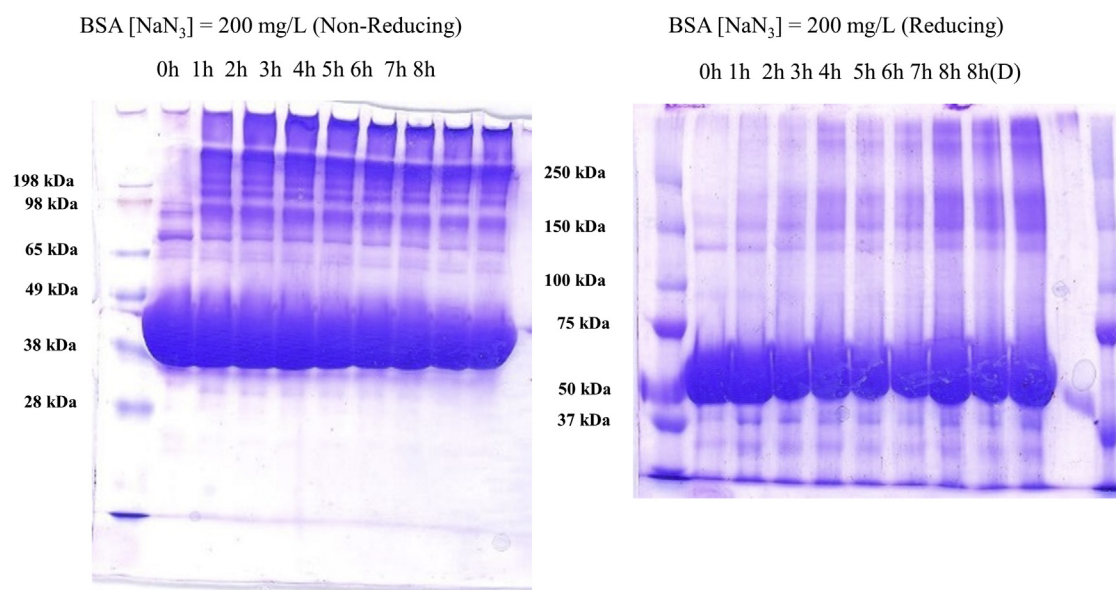

Fig. 5. Polyacrylamide gel electrophoresis of aggregated BSA samples. Far left lane in both gels is a protein ladder standard. (L): Samples run without reducing agent or surfactant (native conditions). (R): Samples run under reducing conditions with β-mercaptoethanol added to the samples and SDS in the running buffer. Sample at 8 h(D) has been diluted to show effect of loading on detection of protein as there was some concentration during the sample preparation. The furthest right lane is standard protein ladder.
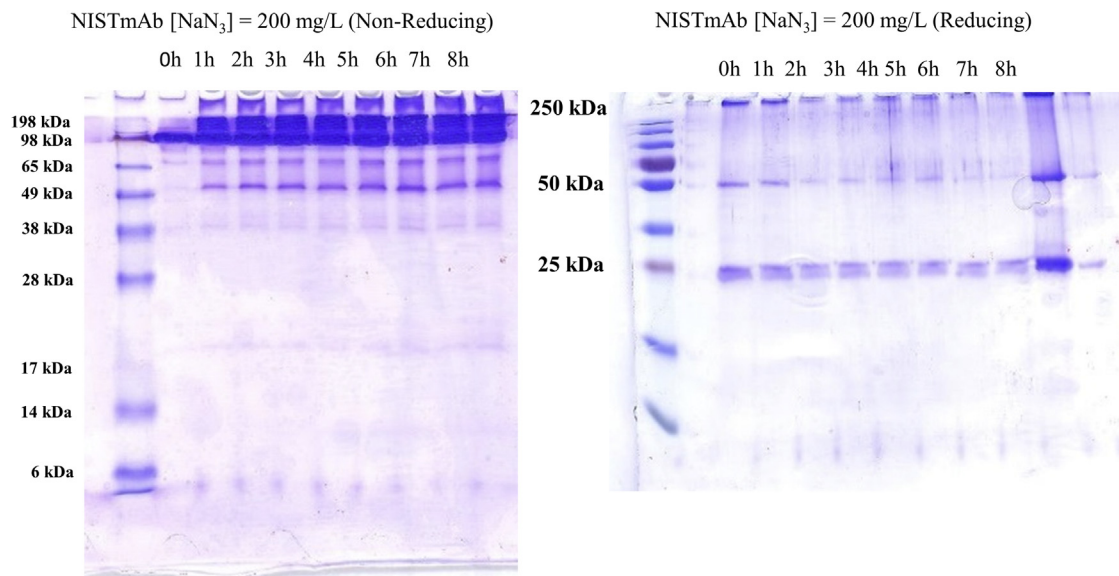
NISTmAb [NaN₃] = 200 mg/L (Non-Reducing)   NISTmAb [NaN₃] = 200 mg/L (Reducing)

Fig. 6. Polyacrylamide gel electrophoresis of aggregated NISTmAb samples. Far left lane in both gels is a protein ladder standard. (L): Samples run without reducing agent or surfactant (native conditions). (R): Samples run under reducing conditions with β-mercaptoethanol added to the samples and SDS in the running buffer.

reversible for NISTmAb. Reduction and alkylation results in complete recapitulation of the individual polypeptide chains that make up the constituent immunoglobulin. Chemical modifications imposed by the reduction and alkylation suggest that the NISTmAb aggregation proceeds through a cysteine-mediated mechanism. The large aggregates are thus held together by disulfide linkages, which are then broken by the reduction and alkylation procedure. The reversible nature, in general, suggests a much different process for the NISTmAb aggregation compared to BSA. It was attempted to analyze the treated samples by AF⁴-MALS as a complimentary approach to the gel electrophoresis reported here. However, due to some unknown factor related to the reduction chemistry, reduced and capped samples injected into the chromatographic system never reached the detector. So AF⁴-MALS data was not collected on these samples.

Aggregation Modelling with the Lumry-Eyring Nucleated Polymerization (LENP) Model

Roberts et al. have authored a series of papers that apply the LENP model to the transformation of monomeric proteins into protein aggregates under a variety of limiting cases and conditions.[20–22] This model has been successfully applied to the aggregation kinetics of a variety of proteins undergoing thermal, pH, ionic strength and buffer composition and freeze/thaw stresses to accelerate the formation of aggregates.[23] Williams and coworkers successfully applied AF⁴-MALS analysis to aggregated IgG protein and used the LENP model to fit the data.[24]

The LENP model was applied to this data to extract the related kinetic quantities. As can be seen in Fig. 4, as the concentration of sodium azide in the NISTmAb samples increases the extent of monomer loss also increases. Concomitantly, the molar masses of the aggregate species increase over time in a way that is azide-concentration dependent. The data point at time zero hours was excluded as the model does not account for aggregation at the initial time point. Experimentally at time zero there is a negligible amount of aggregate that is below a meaningful quantification threshold. Therefore, it was not included in the aggregate analysis as the model intrinsically disregards it. Based on the modeling with

a parameter of three nuclei forming the initial condensed aggregate the model begins around 450 kDa, corresponding directly to this.

There appears to be little difference at low concentrations of azide (*i.e.* 100 mg/L or less) but with a strong effect seen at the higher concentrations (200 mg/L or 400 mg/L). This implicates azide mechanistically in the aggregation mechanism as it directly impacts the both the consumption of the monomer and molar mass of the aggregate. This can generally be explained by the LENP model of aggregation, shown as a generalized scheme in Fig. 7. Briefly, the model consists of native monomeric proteins undergoing multiple reversible processes to form reactive monomer species. These reactive monomer species then form into oligomers that can reversibly disassemble back into unreactive and/or native monomeric proteins. During the formation of reversible oligomers, they can undergo a variety of processes to form (irreversibly) a minimum sized aggregate nucleus. These aggregate nuclei then undergo "chain" or "down-hill" polymerization with the addition of reactive monomer species forming progressively larger and larger protein aggregates. Aggregates can also grow by condensation with other aggregated nuclei. Either of these growth procedures continue until a final irreversible condensation step occurs that essentially stops the aggregate growth.

The LENP model can yield equations describing the concentration of time-dependent change in the concentration of the monomer as well as the evolution of the aggregate molar mass. Both quantities are easily obtained from an AF⁴ separation followed by inline MALS characterization which measures both concentration of the various species in a mixture as well as their molar masses. This application of the LENP model results in a system of three coupled ordinary differential equations (ODEs), which can be regressed to the experimental data. The time dependent change in the monomer concentration is described by Equation (4):

$$\frac{dm}{dt} = -\frac{1}{\tau_n}xm^x - \frac{1}{\tau_g}\delta m^\delta \qquad (4)$$

where m is the concentration of monomer (both native and reactive) divided by the initial monomer concentration, τ_n is the characteristic time to form a nucleus (the inverse of a typical rate constant), x is the nucleation stoichiometry (an integer
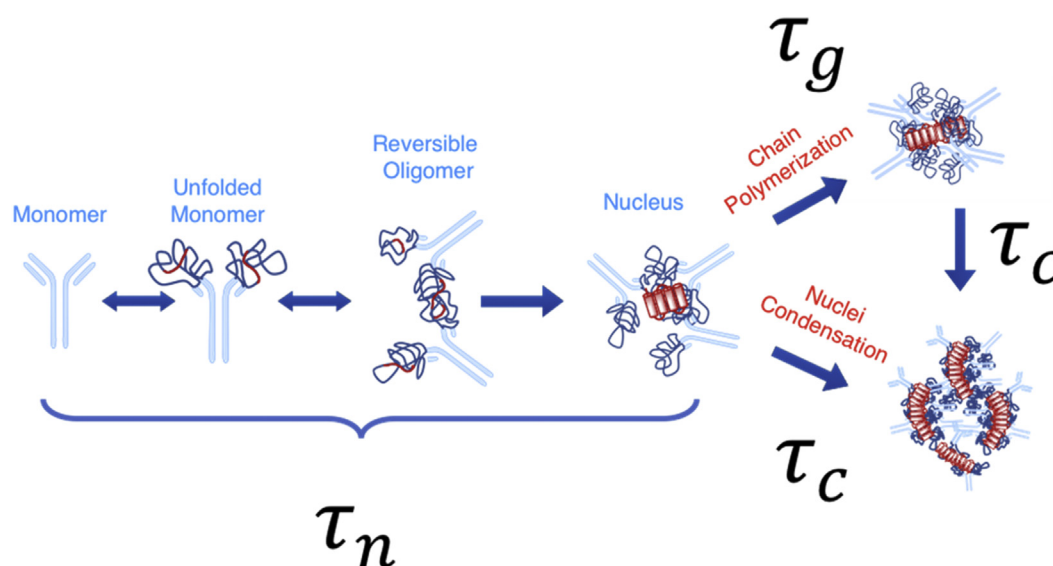
Fig. 7. Pictorial representation of the LENP model of protein aggregation. The processes are described in detail in the text. [Freely adapted from the published literature.][31].

representing the minimum number of monomers required to form an irreversible nucleus), τ_g is the characteristic time of "chain" polymerization, and δ is the integer number of monomers consumed in a given polymerization characteristic time. In practice for proteins, x ranges from 2 to 10 and δ ranges from 1 to 3.[25] In this work, values of x ranging from 2 to 6 and values of δ ranging from 1 to 3 were systematically evaluated. The data were fit with each combination of x and delta values and the fit of the model to the experimental data with the highest correlation ($x = 3$ and $\delta = 1$) were identified and presented. Thus, the values of $x = 3$ and $\delta = 1$ most closely matched the experimental data sets and were used in all subsequent analysis. Given the physical meaning of x and δ, aggregate growth cannot proceed until an irreversible nucleus forms from three reactive monomers. This matches the experimental data where the minimum aggregate in the absence of azide at 1 h of thermomechanical stress yields an aggregated molar mass of around 430 kDa, which is close to the mass of three 150 kDa IgG monomers combined. Once this critical nucleus size is reached, the aggregate grows by addition of single reactive monomers until the growth terminates. The first term in the right-hand side of Eq. (4) describes the loss of monomer due to the formation of irreversible aggregate nuclei, where the rate of nucleus formation is proportional to the term xm^x; this term follows the nucleated polymerization kinetics of actin first described by Osaka and Asakura.[26] Monomer can also be consumed by aggregate growth according to the second term in the right-hand side of Equation (4). The time dependent change in the total amount of aggregate is described by Eq. (5):

$$\frac{d\sigma}{dt} = \frac{1}{\tau_n}m^x - \frac{1}{2\tau_c}\sigma^2 \qquad (5)$$

where σ is the total concentration of reactive aggregate divided by the initial monomer concentration and τ_c is the characteristic time for aggregate condensation. The first term in the right-hand side of Equation (5) shows a growth of reactive aggregate from the formation of new nuclei while the second term show loss due to the irreversible, growth-terminating condensation of monomers. The

evolution of the second moment of the aggregate molar mass distribution, λ_2, with respect to time is described by Equation (6):

$$\frac{d\lambda_2}{dt} = x^2\frac{m^x}{\tau_n} + \frac{1}{\tau_g}m^\delta\left(\delta^2\sigma + 2\delta(1-m)\right) + \frac{1}{\tau_c}(1-m)^2 \qquad (6)$$

Finally, the second moment of the size distribution is related to the weight average molar mass by Equation (7):

$$\frac{M_w^{agg}}{M_w^{mon}} = \frac{\lambda_2}{1-m} \qquad (7)$$

The LENP model has three parameters that are fitted to two data sets: the fraction of free monomer and average molar mass of the aggregate. It should be noted that the equations were fitted to the data in non-dimensional units and then transformed back into physical units. The fits in non-dimensional units were quite good (see Figure S1 in the Supplementary Information for an example of this fit), but in the plots of measured quantities, small errors in the non-dimensional fit are magnified with more rapid formation and larger resulting aggregates found at the higher sodium azide concentrations. The NISTmAb data (both the monomer concentration and the aggregate molar mass) were fit using this coupled ordinary differential equations (ODEs) procedure to produce the data in Table 1 below. The fit of monomer loss matches the experimentally measured data quite well for zero to low concentrations of sodium azide. At higher concentrations, the fit is quantitatively less satisfactory, but still qualitatively matches the data. The fit of aggregate molar masses at short times do not match experimental data, but this is to be expected as the aggregates are oligomeric in nature and have not grown to sufficient size at aggregation times of less than 2 h.

Specifically, nucleation times (τ_n) decrease by over three-fold, going from over 4 h down to just over an hour with increasing azide concentration. In contrast the growth (*i.e.* polymerization) time parameter (τ_g) does not change much with respect to the azide concentration. Perhaps most interestingly the condensation time parameter (τ_c) varies from effectively infinite without azide to just over 2 h as the sodium azide concentration increases.

Based on this result, we conclude that the azide-mediated aggregation of the NISTmAb is strongly affected by the azide concentration as it decisively impacts the nucleation process. Put a

Table 1
Extracted Fitting Parameters with Associated Uncertainties (1σ) for Aggregation of NISTmAb Obtained for the LENP Model Using the Coupled ODEs Described Above.

[NaN$_3$]	x	δ	τ_n(min)	τ_g(min)	τ_c(min)
0 mmol/L	3	1	270 ± 40	39 ± 3	>10,000
1.54 mmol/L (100 ppm)	3	1	190 ± 20	41 ± 3	600 ± 400
3.08 mmol/L (200 ppm)	3	1	120 ± 20	31 ± 2	240 ± 50
6.15 mmol/L (400 ppm)	3	1	80 ± 20	28 ± 2	130 ± 10

different way, increased azide concentration increases the number of reactive nuclei forming from the disordered monomers in the solution. This assertion arises from the noted, systematic decrease in the nucleation time (τ_n) as the azide concentration increases. The shortening of the nucleation time is direct evidence that more nucleation occurs with more azide in solution. This is fundamentally why the aggregation proceeds more rapidly to form aggregates as the azide concentration increases. The generalized lack of dependence on the growth time implies that the azide does not impact the growth rate through chain polymerization and so the growth depends only on the total amount of monomer initially available. Additionally, as the condensation time appears to decrease while the growth time remains constant, we also conclude that the aggregates grow in mass by collision and further aggregation of already formed soluble aggregates. The minimal change in the growth time (τ_g) physically means that the increase in the aggregation kinetics does not occur due to increased addition of free monomers to the growing aggregate. In Fig. 7, the extracted fit parameters therefore suggest that the amount of "chain polymerization" is relatively unaffected by increased azide concentration, whereas the process labeled "nuclei condensation" is strongly dependent on the azide concentration.

Thus, the presence of the azide anion both kinetically facilitates the conversion of reversible oligomers of associated distorted monomers into irreversible aggregate seed nuclei as well as driving aggregate-aggregate association. Increased aggregate-aggregate interactions naturally increase both extent of the aggregation (as measured by the change in monomer concentration) as well as the formation of the higher order molecular weight aggregates (measured by the aggregate molecular weight). This result is in agreement with the work of Bria and Williams, where the aggregation of the IgG was also carried out in the presence of azide at approximately 3 mmol/L concentration.[24] In the absence of azide, the aggregate-aggregate association is negligible, and aggregation proceeds only through the formation of unstable (and irreversible) aggregates of the distorted monomers. Therefore, it can be surmised that the azide has some sort of intrinsic interaction with the antibody that modulates these kinetic processes in solution.

This same kinetic fitting/analysis was unable to fit the LENP model to the BSA experimental data. Therefore, the BSA data (Fig. 2) are presented for the sake of completeness without kinetic analysis or interpretation. The BSA aggregation process does not fit the LENP model of aggregation. Perhaps there is a different mechanism by which the BSA aggregates without the monomer distortion into the reversible aggregates via concurrent chain growth and condensation kinetic steps. One final aspect of note is that we observe no insoluble aggregates for any of the samples (BSA or NISTmAb) at any of the azide concentrations or times measured. This was determined both via optical inspection of the samples as well as calculation of the total protein recovered, as measured by UV spectroscopy. The total mass of protein (*i.e.* monomer plus aggregate) injected across all samples was quantitatively recovered with the amount of total protein injected, as based on the initial prepared stock concentration. Therefore, we concluded that no insoluble aggregates were detected. The LENP model of aggregation predicts at some large

enough molecular weight of the aggregated peptide chains, aggregates will become insoluble at some critical mass in a way that has been observed for neurodegenerative amyloid-like aggregates and other proteins.[27,28] The fact that only soluble sub-micrometer type aggregates were observed implies that aggregation of BSA and NISTmAb may mean that the kinetic process may be limited by the aggregate-aggregate growth which is based on a collisional flux; rather than the addition of monomer to the growing aggregates as envisioned more broadly in chain polymer growth mechanisms. It may also be that there is a "window" of aggregation where soluble aggregates can form and remain in solution indefinitely without the formation of insoluble aggregates. Small variations to the aggregation conditions may tip the proteins out of the "window," and insoluble aggregates would appear.

Possibility of Transition Metal Mediated Process

Redox-active transition metal contaminant(s) in the sodium azide solution used to make the buffer could produce a similar cysteine-based aggregation phenomenon through redox cycling.[29,30] To assess this possibility, the stock solution of sodium azide as received was analyzed by inductively coupled plasma mass spectrometry sweeping across all isotope masses from ^{3}Li to ^{238}U. Not including the expected ^{23}Na, only titanium, nickel and barium were detected in the samples at levels of less than 20 μg/kg, 10 μg/kg and 2 μg/kg, respectively. The stock azide solution is diluted 250-fold during preparation of the buffer and so any detected elements are at even lower levels in the aggregation samples than those measured in the stock solution. Appropriate standard mixes of naturally abundant isotopes were used to calibrate the instrument and assure it was functioning with expected limits of detection in the parts per billion range. In general, this result is not surprising. Sodium azide is typically commercially produced by reacting ammonia gas with elemental sodium, followed by treatment with dinitrogen monoxide (nitrous oxide). Thus, there are very few opportunities for the entrance of transition metals into the azide solution other than some small residual impurities in the elemental sodium that was used. Since most sodium is produced by electrolysis of sodium chloride solutions, a high purity of the sodium can be reasonably expected to be used in the general preparation of the sodium azide. Therefore, it was not expected that there would be any transition metal ions detected in the sodium azide stock solution. It can be said decisively that the observed aggregation is not transition metal mediated.

Implications of Azide in Aggregation Mechanism

Native IgG proteins exist as a tetramer of peptide chains (specifically a dimer of two dimers) that are held together by disulfide bonds between the cysteine residues on the four peptide chains. We suggest that the presence of the azide facilitates protein aggregation through the scrambling or destabilization of the disulfide bridges that maintain the tetrameric structure of the native IgG molecule. The observed differences across both the monomer concentration and the aggregate molecular mass as a function of the azide concentration indicate there is likely some effect of the azide interacting with the amino acid residues of the intact immunoglobulin. However, we do not presently have information on the details of the thermodynamic landscape of the aggregation reaction coordinate.

The reduced form of homocysteine in its cystine disulfide form can act as a weak electrophile. Since the terminal nitrogen of the azide anion is a known weak nucleophile, it is therefore possible that they may cross react. The elevated temperatures used in aggregation studies may enable this reaction to thermodynamically

proceed even though we find no evidence of aggregation for protein solutions stored at 4 °C in the presence of azide. This may be the primary pathway for how and why the aggregation of the NISTmAb was observed. Additionally, it is of note that since BSA is a single polypeptide chain it intrinsically has only intrapeptide strand disulfide bonds. The NISTmAb, on the other hand, has many disulfide bonds contributing to the protein tertiary structure. We suspect that fundamental differences in protein thermodynamic stability (*i.e.* reaction landscape) may be the determinative cause for the differences in the observed aggregation phenomena seen herein, but have no evidence presently.

Conclusions

This report describes a direct study of the effect of azide preservative on the kinetics of purified protein aggregation. We demonstrate that for a monoclonal antibody like NISTmAb, aggregation is both time- and azide-dependent. The BSA aggregates independently of the azide concentration but in a controlled time-dependent manner. The results have been placed into the context of the LENP model for the NISTmAb aggregation, demonstrating that the primary drivers of the antibody aggregation are nucleation of aggregate chains as well as aggregate-aggregate condensation events. This is shown to be directly related to the azide solution concentration. Finally, we show evidence that the NISTmAb aggregation is fully reversible and implicate a cysteine-mediated mechanism in that process. BSA aggregates through a different mechanism and could not be fit under the applied LENP aggregation kinetic model. Finally, we assert that the presence of preservatives like azide does have direct effects on aggregation of proteins of interest and provide a methodology for exploring and exploiting this.

Acknowledgements

Appendix A. Supplementary Data

Supplementary data to this article can be found online at https://doi.org/10.1016/j.xphs.2021.01.013.

References

1. Roberts CJ. Protein aggregation and its impact on product quality. *Curr Opin Biotechnol*. 2014;30:211-217.
2. Kim N, Remmele Jr RL, Liu D, Razinkov VI, Fernandez EJ, Roberts CJ. Aggregation of anti-streptavidin immunoglobulin gamma-1 involves fab unfolding and competing growth pathways mediated by pH and salt concentration. *Biophys Chem*. 2013;172:26-36.
3. Kalonia C, Toprani V, Toth R, et al. Effects of protein conformation, apparent solubility, and protein-protein interactions on the rates and mechanisms of aggregation for an IgG1 monoclonal antibody. *J Phys Chem B*. 2016;120:7062-7075.
4. *Immunogenicity Assessment for Therapeutic Protein Products*. Services, D. o. H. a. H.; 2014.
5. Calloni G, Lendel C, Campioni S, et al. Structure and dynamics of a partially folded protein are decoupled from its mechanism of aggregation. *J Am Chem Soc*. 2008;130:13040-13050.
6. Morris AM, Watzky MA, Agar JN, Finke RG. Fitting neurological protein aggregation kinetic data via a 2-step, Minimal/"Ockham's Razor" model: the finke-Watzky mechanism of nucleation followed by autocatalytic surface growth. *Biochemistry*. 2008;47:2413-2427.
7. Nicoud L, Arosio P, Sozo M, Yates A, Norrant E, Morbidelli M. Kinetic analysis of the multistep aggregation mechanism of monoclonal antibodies. *J Phys Chem B*. 2014;118:10595-10606.
8. Filipe V, Kükrer B, Hawe A, Jiskoot W. Transient molten globules and meta-stable Aggregates induced by brief exposure of a monoclonal antibody IgG to low pH. *J Pharm Sci*. 2012;101:2327-2339.
9. Oliva A, Llabrés M, Fariña JB. Fitting bevacizumab aggregation kinetic data with the finke-Watzky two-step model: effect of thermal and mechanical stress. *Eur J Pharm Sci*. 2015;77:170-179.
10. Man A, Luo H, Levitskaya SV, Macapagal N, Newell KJ. Optimization of a platform process operating space for a monoclonal antibody susceptible to reversible and irreversible aggregation using a solution stability screening approach. *J Chromatogr A*. 2019;100-108.
11. van der Kant R, Karow-Zwick AR, Van Durme J, et al. Prediction and reduction of the aggregation of monoclonal antibodies. *J Mol Biol*. 2017;429:1244-1261.
12. Layne EC, Nason A. Cytochrome C oxidase from azotobacter Vinelandii. *J Biol Chem*. 1958;231:889-898.
13. Zhou P, Liu X, Labuza TP. Moisture-induced aggregation of whey proteins in a protein-buffer model system. *J Agric Food Chem*. 2008;56:2048-2054.
14. Sonawane SK, Ahmad A, Chinnathambi S. Protein-capped metal nanoparticles inhibit tau aggregation in alzheimer's disease. *ACS Omega*. 2019;4:12833-12840.
15. Mangrolia P, Murphy RM. Retinol-binding protein interferes with transthyretin-mediated β-amyloid aggregation inhibition. *Biochemistry*. 2018;57:5029-5040.
16. Schiel JE, Turner A. The NISTmAb reference material 8671 lifecycle management and quality plan. *Anal Bioanal Chem*. 2018;410(8):2067-2078.
17. Borzova VA, Chebotareva NA, Kleymenov SY, Poliansky NB, Muranov KO. Kinetics of thermal denaturation and aggregation of bovine serum albumin. *PLoS One*. 2016;11(4):e0153495.
18. Schiel JE, Blanco M, Formolo T, et al. *NISTmAb Common Technical Document Case Study*. National Institute of Standards and Technology; 2015.
19. Roelfs M, Kroon PC. *tBuLi/Symfit: Symfit 0.5.2 (Version 0.5.2)*. Zenodo; 2019.
20. Andrews JM, Roberts CJ. Non-native aggregation of α-chymotrypsin occurs through nucleation and growth with competing nucleus sizes and negative activation energies. *Biochemistry*. 2007;46:7558-7571.
21. Li Y, Roberts CJ. A lumry-eyring nucleated-polymerization (LENP) model of protein aggregation kinetics 2. Competing growth via condensation- and chain-polymerization. *J Phys Chem B*. 2009;113:7020-7032.
22. Barnett GV, Qi W, Amin S, Lewis EN, Roberts CJ. Aggregate structure, morphology and the effect of aggregation mechanisms on viscosity at elevated protein concentrations. *Biophys Chem*. 2015;207:21-29.
23. Guo J, Yang X-Q, He X-T, et al. Limited aggregation behavior of ß-conglycinin and its terminating effect on glycinin aggregation during heating at pH 7.0. *J Agric Food Chem*. 2012;60:3782-3791.
24. Bria CRM, Jones J, Charlesworth A, Williams SKR. Probing submicron aggregation kinetics of an IgG protein by asymmetrical flow field-flow fractionation. *J Pharm Sci*. 2015;105:31-39.
25. Li Y, Weiss WF, Roberts CJ. Characterizaiton of high-molecular-weight nonnative aggregates and aggregation kinetics by size exclusion chromatography with inline multi-angle laser light scattering. *J Pharm Sci*. 2009;98:3997-4016.
26. Oosawa F, Asakura S. *Thermodynamics of the Polymerization of Protein*. New York: Academic Press; 1975:194.
27. Rosa M, Lopes C, Melo EP, Singh SK, Geraldes V, Rodrigues MA. Measuring and modeling hemoglobin aggregation below the freezing temperature. *J Phys Chem B*. 2013;117:8939-8946.
28. Crespo R, Villar-Alvarez E, Taboada P, Rocha FA, Damas AM, Martins PM. Insoluble off-pathway aggregates as crowding agents during amyloid fibril formation. *J Phys Chem B*. 2017;121:2288-2298.
29. Giles NM, Watts AB, Giles GI, Fry FH, Littlechild JA, Jacob C. Metal and redox modulation of cysteine protein function. *Chem Biol*. 2003;10:677-693.
30. Leal SS, Botelho HM, Gomes CM. Metal ions as modulators of protein conformation and misfolding in neurodegeneration. *Coord Chem Rev*. 2012;256:2253-2270.